

Chapter 4.2



Dysfunctional cerebellar Purkinje cells contribute to autism-like behaviour in Shank2-deficient mice

Saša Peter, Michiel M. ten Brinke, Jeffrey Stedehouder, Claudia M. Reinelt, Bin Wu, Haibo Zhou, Kuikui Zhou, Henk-Jan Boele, Steven A. Kushner, Min Goo Lee, Michael J. Schmeisser, Tobias M. Boeckers, Martijn Schonewille, Freek E. Hoebeek and Chris I. De Zeeuw

Abstract

Loss-of-function mutations in the gene encoding the postsynaptic scaffolding protein SHANK2 are a highly penetrant cause of autism spectrum disorders (ASD) including cerebellum-related motor problems. Recent studies have implicated cerebellar pathology in etiology of ASD. Here, we evaluate the possibility that cerebellar Purkinje cells represent a critical locus of ASD pathophysiology in Shank2-related ASD. Absence of Shank2 impairs both Purkinje cell intrinsic plasticity and induction of long-term potentiation at the parallel fiber to Purkinje cell synapse. Moreover, inhibitory input onto Purkinje cells is significantly enhanced, most prominently in the posterior lobe where simple spike regularity is most affected. Using Purkinje cell-specific Shank2-knockouts, we replicate alterations of simple spike regularity in vivo and establish cerebellar-dependence of ASD-like behavioural phenotypes in motor learning and social interaction. These data highlight the importance of Shank2 for Purkinje cell function, and support a model by which cerebellar pathology is prominent in certain forms of ASD.

Introduction

Autism spectrum disorders (ASD) are neurodevelopmental disease entities primarily defined by deficits in social interaction and repetitive behaviour [Chen et al 2015]. In addition, individuals with autism often suffer from motor skill deficiencies [Kanner 1943], many of which manifest early in the disease [Zwaigenbaum et al 2013]. The aetiology of ASD is complex with reported pathophysiological alterations encompassing multiple brain regions, including the cerebellum [Chen et al 2015]. Cerebellum-related motor symptoms of ASD patients have been observed by impairments in eyeblink conditioning [Oristaglio et al 2013, Sears et al 1994], eye movement abnormalities [Schmitt et al 2014, Takarae et al 2004], general motor learning deficits [Marko et al 2015, Mostofsky et al 2000] as well as balance and postural difficulties [Memari et al 2014, Stins et al 2015]. Patients with cerebellar lesions emerging later in development are often diagnosed with cerebellar cognitive affective syndrome, a condition characterized by deficits in language, executive function and impaired emotions which overlaps considerably with symptoms in ASD [Schmahmann 2010]. Anatomical evidence for cerebellar involvement in ASD includes a decrease in the number of Purkinje cells (PCs) by post-mortem brain histopathological examination [Allen 2005, Bailey et al 1998] and functional connectivity between the cerebellum, and frontoparietal and sensorimotor regions in resting-state fMRI studies of ASD [Stoodley 2014]. Moreover, the cerebellum is among the most prominent brain regions demonstrating high co-expression of ASD-associated genes [Menashe et al 2013].

Emerging data indicate that neurodevelopmental disorders including ASD result from dysfunctional synaptic networks [Grabrucker et al 2011, Zoghbi & Bear 2012]. The postsynaptic density (PSD) in particular represents a critically important proteomic hub for a considerable proportion of neurodevelopmental disease-causing mutations, including ASD [Bourgeron 2015]. A prominent example is the Shank family of postsynaptic scaffolding proteins, which has gained wide attention because of their strong link to ASD [Berkel et al 2010, Durand et al 2007, Leblond et al 2012, Mei et al 2016, Sato et al 2012]. To date, two studies have independently reported generating Shank2 knockout (KO) mice with ASD-like behaviour and abnormal hippocampal processing [Schmeisser et al 2012, Won et al 2012]. However, in addition to the forebrain, Shank2 is also highly expressed in cerebellar PCs [Böckers et al 2004, Boeckers et al 1999b]. Moreover, patients with Shank2-related ASD exhibit motor impairments consistent with cerebellar dysfunction [Leblond et al 2014]. However, the causal influence of cerebellar dysfunction on Shank2-related ASD has never been established.

We therefore used both global germ-line Shank2 knock-out (KO; Shank2^{-/-}) and PC-specific Shank2

KO (L7-Shank2^{-/-}) mouse models to investigate the causal influence of Shank2 on cerebellar function and ASD-related behaviours. Notably, Shank2^{-/-} mice have impairments in plasticity at the parallel fiber (PF) to PC synapse, increased inhibitory input onto PCs, and significant irregularities in PC simple spike activity. Moreover, L7-Shank2^{-/-} mice show deficits in social interaction and exhibit task-specific repetitive behaviour. Together, these results provide novel insight into the pathophysiological mechanisms by which Shank2 mutations cause impairments in cerebellar function that may contribute to ASD.

Results

Reduction of functional cerebellar AMPAR in Shank2^{-/-} mice

A divergent role of the Shank2 scaffolding protein has been hypothesized for PSD function and cellular morphology (Sala et al 2015). To evaluate the morphology of Shank2-deficient postsynaptic specializations along PC dendrites, we quantified the structural characteristics of dendritic spines and PSDs in the distal molecular layer of global Shank2^{-/-} mice using Golgi-Cox staining of PC dendrites and electron microscopy (Fig. 1). Neither spine density (WT: 1.93 ± 0.74 spines/ μ m dendrite; Shank2^{-/-}: 1.82 ± 0.67 spines/ μ m dendrite; $P=0.2$, Mann-Whitney U-test [MWU-test, see Supplementary Table 1 for additional statistics], nor the length (WT: 1.34 ± 0.77 μ m; Shank2^{-/-}: 1.32 ± 0.50 μ m; $P=0.4$, MWU-test) or width of individual spines (WT: 0.72 ± 0.45 μ m; Shank2^{-/-}: 0.71 ± 0.32 μ m; $P=0.9$, MWU-test) was significantly affected (Fig. 1a). In addition, the length (WT: 313.3 ± 97.1 nm; Shank2^{-/-}: 305.3 ± 96.2 nm; $P=0.3$) and thickness of PSDs (WT: 26.2 ± 6.0 nm; Shank2^{-/-}: 26.0 ± 5.3 nm; $P=0.9$) were similar between genotypes (Fig. 1b,c). In contrast, biochemical analysis of cerebellar synaptosomes indicated that global Shank2^{-/-} mice have lowered expression of AMPA receptor subunits GluA1 (WT: 1.00 ± 0.37 ; Shank2^{-/-}: 0.63 ± 0.23 ; $P=0.041$) (Fig. 1d, Supplementary Fig. 1) and GluA2 (WT: 1.00 ± 0.32 ; Shank2^{-/-}: 0.58 ± 0.11 ; $P=0.014$). In addition, we looked into the ASD pathology related cell adhesion molecule neuroligin 3 (Nlgn3), which has been shown to interact with Shank proteins (Bourgeron 2015), but found no significant difference in its expression (WT: 1.00 ± 0.37 ; Shank2^{-/-}: 0.84 ± 0.33 ; $P=0.4$). Together, these findings indicate that Shank2 is not crucial for the morphological differentiation of PC dendritic spines and PSDs, but instead may play an important role in the maintenance of cerebellar GluA1 and GluA2 levels.

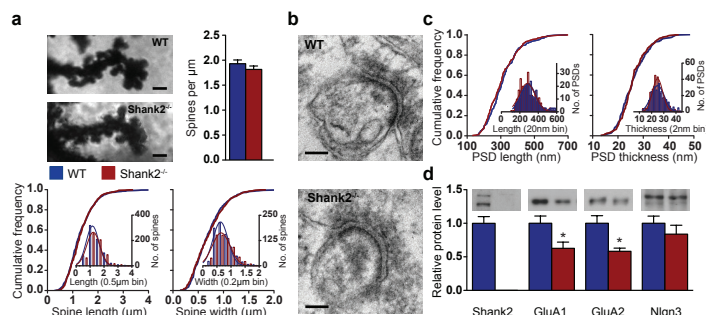


Figure 1. Reduction of AMPA receptor subunits in Shank2^{-/-} cerebellar synaptosomes, but no changes in spine and PSD morphology in the distal molecular layer (DML). (a) Representative images (Golgi-Cox staining) of distal Purkinje cell dendrites in the DML, quantification of spine density (WT, n=97/4, dendrites/mice; Shank2^{-/-}, n=89/4, P=0.2, MWU-test) and cumulative frequency

plots of spine length ($P=0.4$, MWU-test) and thickness ($P=1$, MWU-test) in WT ($n=748/4$ spines/mice) and Shank2^{-/-} mice ($n=639/4$) as indicated. Scale bar: 1 μ m. (b,c) Representative images (electron microscopy) of spine synapses in the DML and cumulative frequency plots of PSD length (WT, $n=226/4$, PSDs/mice; Shank2^{-/-}, $n=243/4$, $P=0.3$) and thickness (WT, $n=223/4$; Shank2^{-/-}, $n=233/4$, $P=0.9$) as indicated. Scale bar: 100 nm. (d) Biochemical analysis of Shank2 (WT, $n=12$ synaptosomes; Shank2^{-/-}, $n=6$), GluA1 (WT, $n=12$ synaptosomes; Shank2^{-/-}, $n=6$, $P=0.041$), GluA2 (WT, $n=11$; Shank2^{-/-}, $n=5$, $P=0.014$), and Nlgn3 (WT, $n=12$; Shank2^{-/-}, $n=6$, $P=0.4$) in cerebellar synaptosomes from WT and Shank2^{-/-} mice as indicated. Data in bar graphs are presented as mean \pm SEM; single asterisks indicates $p < 0.05$.

Normal baseline excitability in Shank2^{-/-} Purkinje cells

Considering that we found a reduction of cerebellar AMPA receptor expression in global Shank2^{-/-} mice, we next examined neurotransmission at the PF-PC synapse using ex vivo whole-cell recordings [at $21 \pm 1^\circ\text{C}$] (Fig. 2a). PF-PC EPSCs, which were obtained in WT and Shank2^{-/-} under comparable conditions [holding current: WT: -389 ± 102 pA; Shank2^{-/-}: -388 ± 114 pA, $P=1$; PC input resistance: WT: 67.2 ± 16.8 M Ω ; Shank2^{-/-}: 69.1 ± 12.4 M Ω ; $P=0.8$; Fig. 2b,c], revealed no significant differences in rise time (WT: 2.1 ± 0.7 ms; Shank2^{-/-}: 1.7 ± 0.6 ms; $P=0.2$) or decay time (WT: 9.7 ± 0.8 ms; Shank2^{-/-}: 9.3 ± 0.3 ms; $P=0.3$) (Fig. 2d,e). Moreover, evoking PF-EPSCs using stimulation currents varying from 3 to 15 μA resulted in similar event amplitudes ($P=0.9$, repeated-measures ANOVA) (Fig. 2f,g) and applying inter-stimulus intervals varying from 50 to 200 ms evoked comparable levels of paired-pulse facilitation ($P=0.2$, repeated-measures ANOVA) (Fig. 2h), indicating that baseline PF-PC synaptic transmission is unaltered by the lack of Shank2. Next, we evaluated whether the loss of Shank2 affected neurotransmission at the climbing fiber (CF) to PC synapse. CF stimulation induced PC complex spikes in WT and Shank2^{-/-}. These waveforms showed no significant differences in the amplitude of the initial Na⁺-spike (WT: 51.8 ± 6.4 mV; Shank2^{-/-}: 48.5 ± 5.9 mV, $P=0.3$) and in the number of subsequent Ca²⁺-spikelets (WT: 1.6 ± 0.5 ; Shank2^{-/-}: 2.0 ± 0.7 ; $P=0.2$) or the amplitude of Ca²⁺-spikelets (WT: 31.8 ± 11.9 mV; Shank2^{-/-}: 33.9 ± 6.4 mV, $P=0.7$) (Supplementary Fig. 2a-c). Moreover, at P9-10 virtually all PCs of both WT and Shank2^{-/-} were innervated by multiple CFs, while at P25-35 all converted into mono-innervation (number of CF responses P9-10: WT: 2.0 ± 0.5 ; Shank2^{-/-}: 2.3 ± 0.5 ; $P=0.2$; P25-35: WT: 1.0 ± 0.0 ; Shank2^{-/-}: 1.0 ± 0.0 ; $P=1$, MWU-test) (Supplementary Fig. 2d,e). Finally, the characteristic

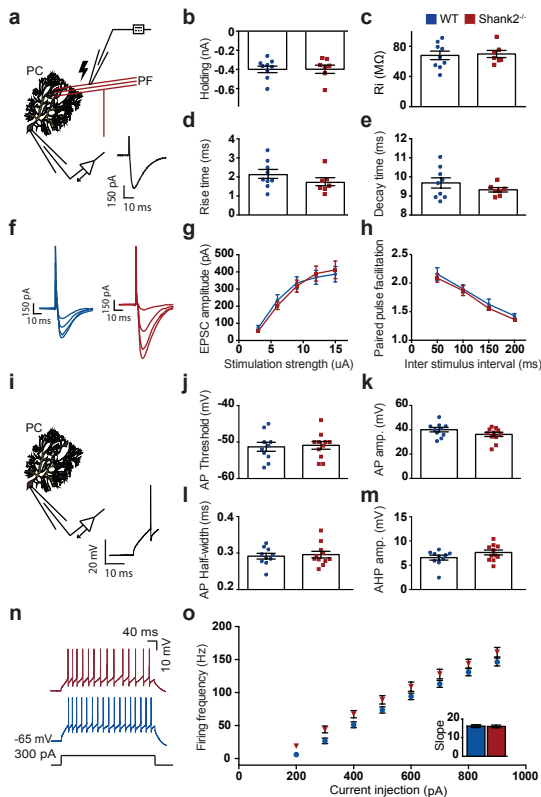


Figure 2. No changes in excited synaptic and intrinsic properties in Shank2^{-/-} Purkinje cells ex vivo. (a) Recording configuration for voltage clamp recordings of PF-PC synaptic transmission. Inset: an example PF-EPSC. [b-e] With comparable holding current [at -65 mV] ($P=1$) and input resistance [Ri] ($P=0.8$), PC EPSC rise time ($P=0.2$) and EPSC decay time ($P=0.3$) are not different between WT ($n=9/6$, cells/animals) and Shank2^{-/-} ($n=7/6$). (f) Example EPSCs in response to 3, 6, 9, 12, and 15 μA stimulation. (g,h) Varying stimulation strength ($P=0.9$, repeated-measures ANOVA) and inter-stimulus interval ($P=0.2$, repeated-measures ANOVA) evoked comparable EPSC amplitude or facilitation (WT, $n=11/3$; Shank2^{-/-} 15/3). (i) Recording configuration for whole cell recording. Inset: an example action potential. (j-m) Action potential threshold ($P=0.8$), amplitude ($P=0.1$), half-width ($P=0.7$), and afterhyperpolarization ($P=0.2$) were not different (WT, $n=10/6$; Shank2^{-/-}, $n=11/6$). (n) Example traces of intrinsic Purkinje cell excitability as apparent from action potential firing evoked by 300 pA current injections. (o) No difference in evoked firing frequency relative to various levels of current injections (WT, $n=10/5$; Shank2^{-/-}, $n=11/5$, $P=0.1$, repeated-measures ANOVA). Inset barplot shows average slope of firing rate per current step ($P=1$). Data are represented as mean \pm SEM. Two-sided t-tests were used, unless stated otherwise.

paired-pulse depression of CF-PC synaptic transmission showed no differences throughout the tested developmental stages (P9-10: WT: 0.59 ± 0.14 ; Shank2^{-/-}: 0.54 ± 0.11 ; $P=0.5$; P25-35: WT: 0.75 ± 0.11 ; Shank2^{-/-}: 0.77 ± 0.1 ; $P=0.6$) (Supplementary Fig. 2f,g), together indicating that the CF to PC input in Shank2^{-/-} mice is not only normal in its baseline characteristics but also with respect to developmental elimination (Hashimoto & Kano 2003).

To examine PC kinetics, we evoked action potentials (APs) using depolarizing current steps at near-physiological temperature ($33 \pm 1^\circ\text{C}$) (Fig. 2i). Evoked APs showed comparable thresholds (WT: -51.4 ± 3.9 mV; Shank2^{-/-}: -51.0 ± 3.5 mV; $P=0.8$), amplitudes (WT: 39.8 ± 5.8 mV; Shank2^{-/-}: 35.9 ± 5.8 mV; $P=0.1$) and half-widths (WT: 0.29 ± 0.02 ms; Shank2^{-/-}: 0.30 ± 0.03 ms; $P=0.7$), as well as after-hyperpolarization amplitudes (WT: 6.5 ± 1.6 mV; Shank2^{-/-}: 7.5 ± 1.7 mV; $P=0.2$) (Fig. 2j-m). In addition, PC intrinsic excitability was normal (Schonewille et al 2010) in that current step injections of increasing amplitude resulted in a linear current-to-firing frequency relationship ($P=0.1$, repeated-measures ANOVA) (Fig. 2n,o) with a similar slope (WT: 16.2 ± 2.2 Hz; Shank2^{-/-}: 16.1 ± 2.3 Hz; $P=1.0$) (Fig. 2o). Together, these findings indicate that both the baseline transmission at PC excitatory synapses and PC intrinsic excitability remain intact in global Shank2^{-/-} mice.

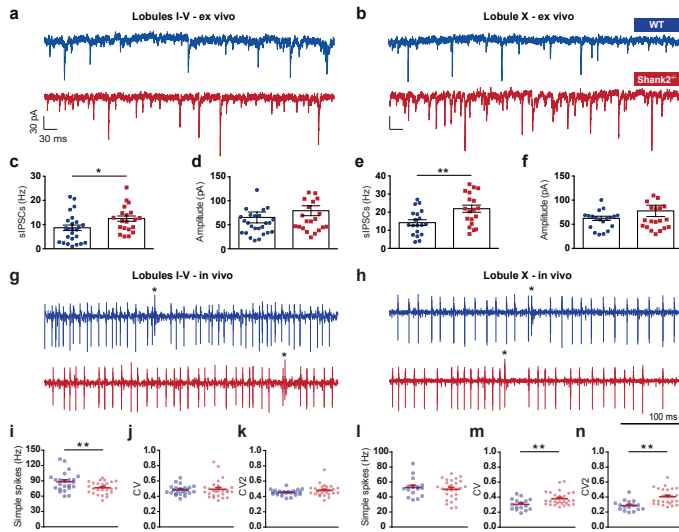


Figure 3. Increased spontaneous inhibitory events and higher simple spike irregularity in Shank2^{-/-} Purkinje cells. (a, b) Example of spontaneous firing inhibitory post synaptic currents (sIPSCs) in lobules I-V and X. (c,e) A higher frequency of sIPSCs is found in both anterior (I-V) ($P=0.0295$) and posterior (X) lobules ($P=0.0079$) in Shank2^{-/-} PCs (anterior: WT, $n=25/3$, cells/animals; Shank2^{-/-}, $n=20/3$; posterior: WT, $n=19/3$; Shank2^{-/-}, $n=19/3$). (d, f) There were no significant differences in sIPSC amplitudes anteriorly ($P=0.1$) or posteriorly ($P=0.5$). (g,h) Extracellular traces of PCs recorded in anterior (left) and posterior (right) lobules in the cerebellum, in WT and Shank2^{-/-}. Asterisks denote complex spikes. (i,j,k) Simple spike (SS) firing frequency was significantly lower ($P=0.0096$) in Shank2^{-/-} ($n=26/3$) compared to wildtype ($n=23/3$), whereas the coefficient of variation (CV) ($P=0.7$) and CV2 ($P=0.1$) did not differ. (l,m,n) In posterior lobule X, while SS firing frequency was similar ($P=0.6$), CV ($P=0.0086$) and CV2 ($P=0.0003$) were significantly higher in Shank2^{-/-} ($n=27/3$) compared to WT ($n=16/3$). Data are represented as mean \pm SEM. Single and double asterisks indicate $P<0.05$ and $P<0.01$, respectively. Two-sided t-tests were used, unless stated otherwise.

Increased sIPSCs and spiking irregularity in Shank2^{-/-} PCs

To investigate inhibition of PCs in global Shank2^{-/-} mice, we recorded spontaneous inhibitory postsynaptic currents (sIPSCs). Since PC activity can be related to the presence or absence of the glycolytic enzyme aldolase-c (referred to as zebrin) (Zhou et al 2014), we recorded from the predominantly zebrin-negative anterior lobules I-V as well as the predominantly zebrin-positive posterior lobule X of the cerebellar cortex (Fig. 3a,b). In both regions, we observed an increase in the frequency (lobules I-V: WT: 8.3 ± 5.9 Hz; Shank2^{-/-}: 12.2 ± 5.4 Hz; $P=0.0295$; lobule X: WT: 14.2 ± 7.0 Hz; Shank2^{-/-}: 21.5 ± 8.8 Hz; $P=0.0079$) (Fig. 3c,e), but not in the amplitude (for lobules I-V, WT: 53.2 ± 24.4

pA; Shank2^{-/-}: 65.2 ± 29.5 pA; P=0.1; for lobule X, WT: 58.9 ± 19.0 pA; Shank2^{-/-}: 64.0 ± 24.7 pA; P=0.5), of sIPSCs (Fig. 3d,f). Importantly, Shank2^{-/-} sIPSC frequency was higher in lobule X than in the anterior lobe (P=0.0002). Given that inhibition decreases the firing frequency of PCs, but increases their irregularity (Häusser & Clark 1997, Wulff et al 2009), we hypothesized that the increased frequency of sIPSCs in Shank2^{-/-} would translate into an overall decrease of in vivo simple spike (SS) activity but with an increased irregularity (Fig. 3g,h). The global Shank2^{-/-} mice did indeed exhibit a decrease in firing frequency in lobules I-V (WT: 88.2 ± 18.7 Hz; Shank2^{-/-}: 76.3 ± 11.8 Hz; P=0.0096) (Fig. 3i), but notably not in lobule X (WT: 52.6 ± 12.7 Hz; Shank2^{-/-}: 50.3 ± 12.9 Hz; P=0.6) (Fig. 3l). Conversely, and consistent with the relative magnitude of the change in sIPSC frequency, the irregularity of PC SS firing was increased in lobule X (CV: WT, 0.30 ± 0.08; Shank2^{-/-}, 0.38 ± 0.09, P=0.0086; CV2: WT, 0.29 ± 0.07; Shank2^{-/-}, 0.40 ± 0.11, P=0.0003), but not in lobules I-V (CV: WT, 0.48 ± 0.06; Shank2^{-/-}, 0.49 ± 0.12, P=0.7; CV2: WT, 0.45 ± 0.04; Shank2^{-/-}, 0.48 ± 0.08, P=0.1) (Fig. 3j-n). The complex spike frequency and the pause in SS firing following each complex spike was similar between global Shank2^{-/-} mice and their WT littermates in both the anterior (WT: frequency 1.28 ± 0.29 Hz; pause 9.11 ± 1.98 ms; Shank2^{-/-}: 1.32 ± 0.24 Hz; 10 ± 2.9 ms; P=0.7 and P=0.2, respectively) and posterior lobules (WT: frequency 0.67 ± 0.19 Hz; pause 19.7 ± 5.5 ms; Shank2^{-/-}: frequency 0.84 ± 0.37 Hz; pause 17.61 ± 5.29 ms; P=0.1 and P=0.2, respectively) (Supplementary Fig. 3). Thus, in the absence of Shank2, the zebrin-positive lobule X selectively exhibits a highly irregular pattern of PC simple spike firing, which is consistent with a relative increase of inhibitory input onto lobule X PCs.

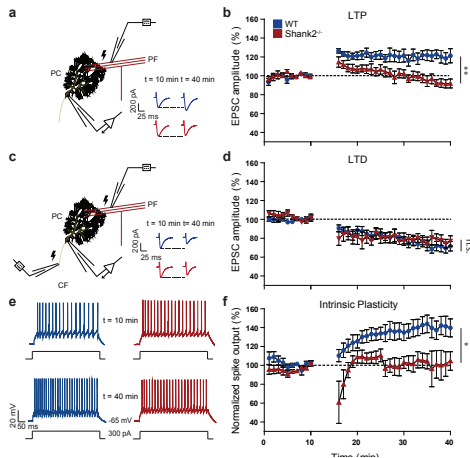


Figure 4. Impaired synaptic and intrinsic plasticity in Shank2^{-/-} ex vivo. (a) Recording configuration for PF-LTP experiments. Inset: example of 5 averaged EPSCs for WT (blue) and Shank2^{-/-} (red) before LTP induction (at 10 minutes) and after LTP induction (at 40 min). (b) LTP experiment with 5 min PF stimulation at 1Hz inducing LTP in WT (n=7/6, cells/animals, P=0.0027) but not in Shank2^{-/-} PCs (n=12/6, P=0.3), which is reflected in the difference between genotypes (P=0.0066). (c) Recording configuration for PF-LTD experiments. Inset: example traces as in a. (d) LTD is induced in both WT (n=9/6, P<0.0001) and Shank2^{-/-} (n=7/6, P=0.0009) PCs, to a similar degree (P=1). (e) Example of traces for intrinsic plasticity with current injections of 300 pA. (f) LTP induction protocol induced enhanced spike output in WT PCs (n=5/4, P=0.0053), but not in Shank2^{-/-} PCs (n=5/4, P=0.5), as reflected in their difference (P=0.0201). Data are represented as mean ± SEM. Single and double asterisks indicate P<0.05 and P<0.01, respectively. All tests were repeated-measures ANOVAs.

Impaired synaptic and intrinsic plasticity in Shank2^{-/-} PCs

Given that Shank2 functions as a PSD scaffolding protein of postsynaptic receptors (Grabrucker et al 2011, Sala et al 2015) for which we observed decreased expression of both GluA1 and GluA2 in cerebellar synaptosomes of Shank2^{-/-} mice (Fig. 1), we reasoned that PC synaptic plasticity might also be affected (Schmeisser et al 2012, Won et al 2012). Induction of long-term potentiation (LTP) [33 ± 1 °C; 1 Hz, 5 min PF-tetanus] (Fig. 4a) reliably increased PF-EPSC amplitudes in WT PCs [121.1 ± 19.8% at t=40 min; P=0.003, repeated-measures ANOVA], but not in those of global Shank2^{-/-} mice [91.8 ± 14.2% at t=40; P=0.3, repeated-measures ANOVA] (Fig. 4b). In contrast, both WT and global Shank2^{-/-} mice exhibited robust long-term depression (LTD) of PF-EPSCs following co-activation [1 Hz] of PFs and CFs (WT: 71.4 ± 14.9%; P<0.0001; Shank2^{-/-}: 76.9 ± 14.6%; P=0.0009, repeated-

measures ANOVA) [Fig. 4c,d]. Since LTP has been reported to facilitate adaptation of intrinsic properties, driving spike activity [Schonewille et al 2010], we next examined PC intrinsic plasticity before and after PF-LTP induction [Fig. 4e]. Whereas WT mice readily demonstrated a potentiation of intrinsic excitability ($139.7 \pm 21.3\%$ at $t=40$ min; $P=0.005$, repeated-measures ANOVA), intrinsic plasticity was markedly impaired in global Shank2^{-/-} mice ($104.6 \pm 22.2\%$ at $t=40$ min; $P=0.5$, repeated-measures ANOVA) [Fig. 4f]. These results suggest that Shank2 is a critical modulator of both synaptic and intrinsic plasticity in Purkinje cells.

Expression of Shank2 in L7-Shank2^{-/-} mice

To explore the behavioural impact of the lack of Shank2 in PCs, we generated a PC-specific knockout of Shank2 [see methods section] using the floxed version of the Shank2^{-/-} mutants [Schmeisser et al 2012] and the L7-vector [Schonewille et al 2010]. Immunocytochemical analysis with the SA5193 rabbit primary Shank2 antibody [Boeckers et al 1999a, Schmeisser et al 2012] confirmed that Shank2^{-/-} was specifically deleted in PCs in the PC-specific L7-Shank2^{-/-} mice, but not in WT littermates, whereas it was ubiquitously deleted in the global Shank2^{-/-} [Fig. 5]. Importantly, PC-specific deletion of Shank2 had no discernible impact on cellular zebrin identity, or on the zonal patterns of zebrin staining across cerebellar modules [Supplementary Fig. 4].

Impaired motor learning in L7-Shank2^{-/-} mice

Given the variety of electrophysiological aberrations in PCs in the global Shank2^{-/-}, we next examined motor behavior in the PC-specific L7-Shank2^{-/-} mice. Unlike the hyperactivity exhibited by global Shank2^{-/-} mice in an open field [Schmeisser et al 2012, Won et al 2012], mice with PC-specific deletion of Shank2 exhibited no evidence of hyperactivity in the open field test compared to their WT littermates [velocity: WT: 12.28 ± 2.79 cm/s; L7-Shank2^{-/-}: 13.24 ± 2.61 cm/s; $P=0.3$; distance moved: WT: 7.37 ± 1.68 m; L7-Shank2^{-/-}: 7.94 ± 1.57 m; $P=0.3$] [Supplementary Fig. 5a,b]. The lack of hyperactivity was confirmed using the PhenoTyper Box [Noldus], in which free exploration was quantified over a 30 min-period in a homecage-like environment [velocity: WT: 6.7 ± 1.1 cm/s; L7-Shank2^{-/-}: 6.3 ± 1.3 cm/s; $P=0.5$, distance moved: WT: 384.6 ± 68.8 cm; L7-Shank2^{-/-}: 371.7 ± 79.7 cm; $P=0.5$, repeated-measures ANOVA] [Supplementary Fig. 5c,d]. Moreover, during the ErasmusLadder test [Veloz et al 2014] motor performance was similar between genotypes, including the efficiency and timing of steps [2nd day efficiency, WT: $33.1 \pm 20.0\%$; L7-Shank2^{-/-}: 47.1 ± 15.4 cm; $P=0.3$; 2nd day timing: WT: 359.2 ± 84.2 ms; L7-Shank2^{-/-}: 330.7 ± 49.4 ms; $P=0.8$, repeated-measures ANOVA] [Supplementary Fig. 5e,f]. Finally,

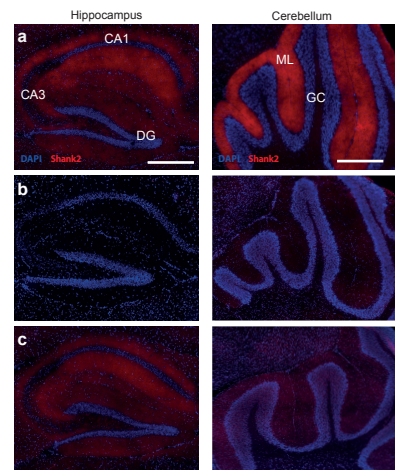


Figure 5. Immunohistological staining of the Shank2 protein in Shank2^{-/-} and L7-Shank2^{-/-} hippocampus and cerebellum. (a) Sagittal cryosection of hippocampal Shank2 (red) and nucleus staining (DAPI; blue) in a WT (left) L7-Shank2^{-/-}. Scale bar: 500 μ m. Sagittal cryosection of cerebellar Shank2 staining (right). Scale bar: 200 μ m. (b) Staining for Shank2 in the hippocampus and cerebellum of the global Shank2^{-/-} shows absence of expression. (c) The L7-Shank2^{-/-} shows expression in the hippocampus, but not in the molecular layer of the cerebellum.

the amplitude [gain] and timing [phase] of baseline optokinetic (OKR) (OKR gain, $P=0.6$, OKR phase, $P=0.9$, repeated-measure ANOVA) and vestibulo-ocular reflexes (VOR) (VOR gain, $P=0.4$, VOR phase, $P=0.2$, repeated-measure ANOVA) were also similar (Supplementary Fig. 5g-j), further highlighting that motor performance is normal in L7-Shank2^{-/-} mutants.

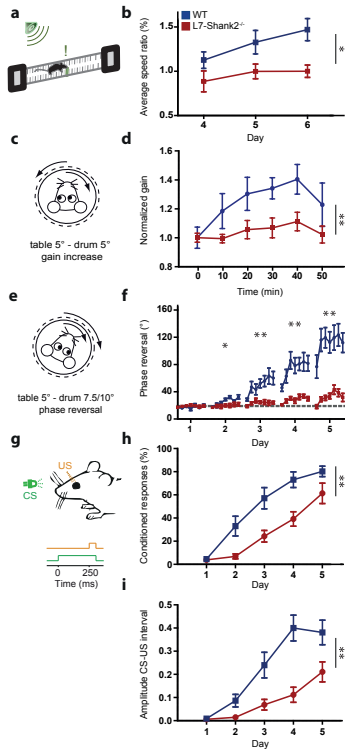


Figure 6. L7-Shank2^{-/-} mice show impaired motor learning. (a, b) After three days of training, WT ($n=9$) but not L7-Shank2^{-/-} mice ($n=6$) ($P=0.018$) learned to increase their speed during a conditioned ErasmusLadder test using tone-cued rung displacements. (c, d) In vestibulo-ocular reflex (VOR) gain increase training, L7-Shank2^{-/-} mice ($n=8$) were not able to adapt their gain like WT mice did ($n=7$) ($P=0.006$). (e, f) L7-Shank2^{-/-} mutants ($n=9$) did not adapt their VOR phase following a reversal training paradigm, whereas WT ($n=9$) did [2nd day, $P=0.047$; 3rd, $P=0.0013$; 4th, $P<0.0001$; 5th, $P=0.0003$]. (g, h, i) Impaired percentage [$P=0.0013$] and amplitude [$P=0.0009$] of conditioned responses (CRs) in L7-Shank2^{-/-} mice ($n=10$) compared to WT ($n=11$) in an eyeblink conditioning paradigm (200 paired trials daily). Data are represented as mean \pm SEM. Single and double asterisks indicate $P<0.05$ and $P<0.01$, respectively. All tests were repeated-measures ANOVAs.

In contrast, motor learning was consistently affected in a variety of cerebellar motor learning tasks (Fig. 6). Using a conditioning task within the ErasmusLadder, in which mice were presented with a tone preceding the elevation of an obstructive rung at a 200 ms interval (Veloz et al 2014), L7-Shank2^{-/-} mice were unable to successfully avoid the obstacle (L7-Shank2^{-/-} versus WT: $P=0.018$, repeated-measures ANOVA) (Fig. 6a,b). Furthermore, L7-Shank2^{-/-} mice failed to acquire the normal increase in VOR gain [L7-Shank2^{-/-} versus WT: $P=0.006$, repeated-measures ANOVA] or shift in VOR phase (2nd day; $P=0.047$, 3rd $P=0.0013$, 4th $P<0.0001$, 5th $P=0.0003$, repeated-measures ANOVA) following visuovestibular mismatch training (De Zeeuw & Ten Brinke 2015) (Fig. 6c-f). Finally, L7-Shank2^{-/-} mice exhibited a significant impairment of Pavlovian eyeblink-conditioning (ten Brinke et al 2015) using a light pulse as the conditioning stimulus (CS) and a corneal air puff as the unconditioned stimulus at a 250 ms interval (conditioned response or CR rate: $P=0.0013$; CR amplitude: $P=0.0009$; repeated-measures ANOVA) (Fig. 6g-i). These findings indicate that L7-Shank2^{-/-} mice have normal baseline motor performance, but prominent impairments in motor learning.

Irregular in vivo PC simple spikes in L7-Shank2^{-/-} mice

To investigate whether the changes in electrophysiological properties observed in PCs of the global Shank2^{-/-} mice may contribute to the behavioural phenotypes observed, we tested to what extent the changes in simple spike activity also occurred in the L7-Shank2^{-/-} mice. We first recorded extracellular single units in vivo from the largely zebrin-negative lobules I-V (Fig. 7a-d) and the predominantly zebrin-positive lobules IX-X (Fig. 7e-h). Importantly, the recordings in the L7-Shank2^{-/-} mice fully reproduced the increases in CV (WT, 0.35 ± 0.07 ; L7-Shank2^{-/-}, 0.49 ± 0.09 ; $P<0.0001$) and CV2 (WT, 0.36 ± 0.06 ; L7-Shank2^{-/-}, 0.47 ± 0.06 ; $P<0.0001$) (Fig. 7g,h) that were found in the posterior lobules of the global Shank2^{-/-} (Fig. 3i-n), confirming the higher SS irregularity. In addition, the L7-Shank2^{-/-} mice also showed signs of SS irregularity in the anterior lobules in that their CV2 was also significantly increased (WT, 0.43 ± 0.04 ; L7-Shank2^{-/-}, 0.47 ± 0.04 ;

$P=0.0092$] [Fig. 7c,d]. The L7-Shank2^{-/-} SS mice activity did not show higher firing frequencies in either the anterior (WT: 104.4 ± 25.8 Hz; L7-Shank2^{-/-}: 101.2 ± 19.7 Hz; $P=0.6$) or posterior (WT: 70.9 ± 19.5 Hz; L7-Shank2^{-/-}: 76.3 ± 23.4 Hz; $P=0.4$) lobules [Fig. 7b,f]. Finally, we also recorded SS activity of PCs in the flocculus of the vestibulocerebellum, because they are known to directly control VOR adaptation [Wulff et al 2009] [Fig. 7i-l]. In PCs that were identified to be related to VOR-adaptation by their response to motion around the vertical axis in space, we again found a significant increase in SS irregularity (CV: WT, 0.39 ± 0.07 ; L7-Shank2^{-/-}, 0.53 ± 0.08 ; $P<0.0001$; CV2: WT, 0.39 ± 0.07 ; L7-Shank2^{-/-}, 0.52 ± 0.08 ; $P<0.0001$), while their overall firing frequency was unaffected (WT: 68.2 ± 15.0 Hz; L7-Shank2^{-/-}: 69.6 ± 18.8 Hz; $P=0.8$) [Fig. 7j-l]. Moreover, L7-Shank2^{-/-} showed a bigger difference with WT in SS irregularity in the posterior lobules (40.0% and 30.6% higher CV and CV2, respectively) compared to that in the anterior lobules (4.4% and 9.3% higher CV and CV2, respectively). No significant differences were observed in the duration of the complex spike-induced simple spike pause or the complex spike firing frequency in any of the recorded lobules ($P>0.2$ in all cases) [Supplementary Fig. 6]. Together, L7-Shank2^{-/-} mice demonstrate the critical importance of Shank2 in PCs for maintaining SS regularity.

Reduced cognitive functioning in L7-Shank2^{-/-} mice

We next examined social and repetitive ASD-like behaviours in the PC-specific L7-Shank2^{-/-} mice. The three-chamber social interaction task is a widely used social interaction paradigm for evaluating ASD-like behaviour in mouse models of autism [Schmeisser et al 2012, Won et al 2012]. WT mice exhibited a normal preference for the chamber in which the stranger mouse [S1] was present, compared to the empty chamber ($P=0.0002$, MWU-test) [Fig. 8a]. In contrast, L7-Shank2^{-/-} mice had no preference for either S1 or the empty chamber ($P=0.7$, MWU-test) [Fig. 8b]. Comparing the preference index [stranger-empty] between WT and L7-Shank2^{-/-} mice revealed a significantly decreased preference of L7-Shank2^{-/-} mice for the stranger mouse ($P=0.0213$) [Fig. 8c], indicating their social interaction deficits. With the introduction of a second stranger in the previously empty chamber, WT mice again demonstrated an increased preference for the novel stranger [S2], this time compared to the familiar mouse [S1] ($P=0.0001$, MWU-test) [Fig. 8d], whereas L7-Shank2^{-/-} mice showed no preference for either the familiar or the novel stranger mice ($P=0.1$, MWU-test) [Fig. 8e]. Comparing the preference index [S2-S1] between WT and L7-Shank2^{-/-} confirmed the

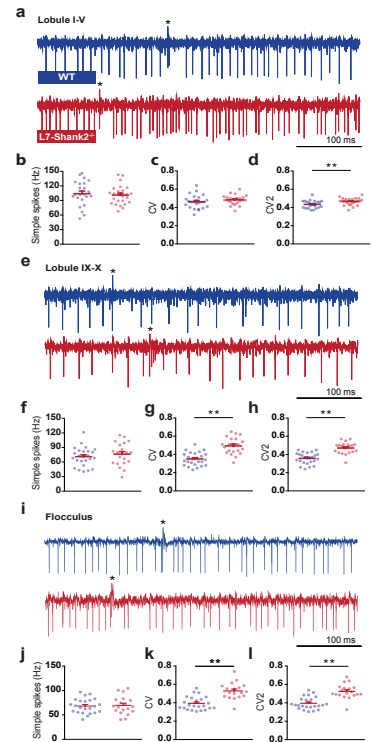


Figure 7. In vivo simple spike firing characteristics in L7-Shank2^{-/-} Purkinje cells. (a) Extracellular PC traces recorded from anterior lobules [I-V] in WT (top) and L7-Shank2^{-/-} (bottom) mice. (b,c,d) Firing characteristics in the anterior lobules reveal a difference in CV2 ($P=0.0092$) between L7-Shank2^{-/-} ($n=25/3$, cells/animals) and WT ($n=23/3$). (e) Example PC traces from posterior lobules [IX-X]. (f,g,h) PCs from the posterior cerebellum in L7-Shank2^{-/-} ($n=21/3$) showed significantly higher CV ($P<0.0001$) and CV2 ($P<0.0001$) values compared to WT ($n=25/3$). (i) Example PC traces from posteriorly located flocculus, which is responsible for VOR learning. (j,k,l) Again, L7-Shank2^{-/-} ($n=19/2$) shows significantly higher CV ($P<0.0001$) and CV2 ($P<0.0001$) values than WT ($n=23/2$). Double asterisks denote $P<0.01$.

impairment of social interaction in L7-Shank2^{-/-} mice ($P=0.0136$) (Fig. 8f). Because of previously reported compulsive grooming (Schmeisser et al 2012) and jumping (Won et al 2012) in global Shank2^{-/-} mice, we next examined repetitive behaviour. We observed no significant differences between WT and L7-Shank2^{-/-} mice in the percentage of buried marbles in the marble-burying task ($P=1.0$) (Fig. 8g) or in the duration of grooming over a 15 min-period ($P=0.054$) (Fig. 8h). However, the L7-Shank2^{-/-} mice did show an increase of repetitive behaviour in the T-maze through an increased perseveration, highlighting a reduction in cognitive flexibility ($P=0.0023$, MWU-test) (Fig. 8i). Finally, we observed no significant difference in anxiety ($P=0.7$, χ^2 -test) or olfactory sensitivity ($P=0.6$) of L7-Shank2^{-/-} mice that could have potentially biased the social behaviour assessments (Supplementary Fig. 7). Together, these results indicate that L7-Shank2^{-/-} mice exhibit ASD-like social impairments and task-specific repetitive behaviour.

Discussion

Severe loss-of-function mutations in SHANK2 have been firmly established as conferring a high genetic risk for ASD and intellectual disability (Berkel et al 2010, Leblond et al 2012, Leblond et al 2014). Children with disruptive SHANK2 mutations exhibit motor impairments, language delay and cerebellar dysfunction including dysmetria and dysdiadochokinesis (Leblond et al 2014). Considering the increasing evidence for cerebellar involvement in ASD (Becker & Stoodley 2013), we investigated anatomical, molecular and physiological consequences of global Shank2 ablation in the cerebellum. In addition, we analyzed L7-Shank2^{-/-} mice with cerebellar PC-specific deletion of Shank2 to evaluate the extent to which the ASD-related behavioural findings in global Shank2^{-/-} mice can be attributed to cerebellar dysfunction.

In recent years, several genetic mouse models for ASD have been used for the study of cerebellar abnormalities. The first study to implement a Purkinje cell-specific model related to ASD involved the deletion of FMR1, the fragile X mental retardation 1 protein (Koekkoek et al 2005). In this study, the authors reported eye-blink abnormalities and increased LTD in both global and Purkinje cell-specific deletion of FMR1. Furthermore, global Nlgn3-KO mutants exhibited deficits in cerebellum-related motor

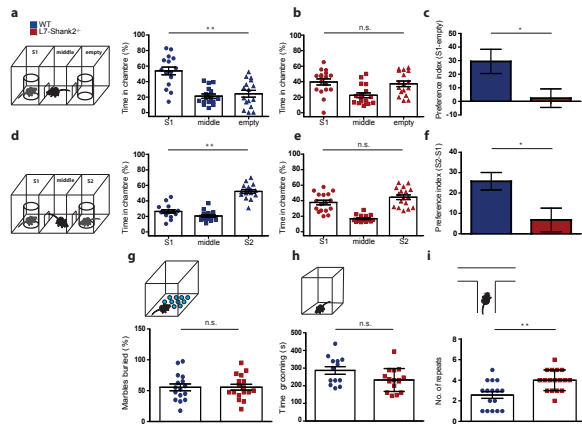


Figure 8. L7-Shank2^{-/-} mice show social impairment and signs of task-specific repetitive behaviour. [a] Three-chamber social interaction evaluated by relative time spent in each chamber. WT ($n=16$) prefer to spend time in the room with the stranger 1 mouse [S1], compared to the empty room ($P=0.0002$, MWU-test). [b] This was not the case for L7-Shank2^{-/-} ($n=17$) mice ($P=0.7$, MWU-test). [c] The preference index [S1-empty] confirms the difference between genotypes ($P=0.021$). [d] Following the introduction of a second stranger [S2], WT ($n=16$) prefer to spend time in the chamber with S2 compared to that with S1 ($P=0.0001$, MWU-test). [e] The L7-Shank2^{-/-} mice ($n=17$) did not show a preference for newly introduced S2 ($P=0.1$, MWU-test). [f] The S1-S2 preference index indicates that WT prefer S2 more than L7-Shank2^{-/-} do ($P=0.013$). [g] No difference was found in a marble burying task indicative of anxious and/or repetitive behaviour (WT, $n=16$; L7-Shank2^{-/-}, $n=17$, $P=1.0$). [h] L7-Shank2^{-/-} ($n=16$) seemed to trend towards less grooming than WT ($n=13$) ($P=0.054$). [i] T-maze paradigm showed less consecutive alternations in L7-Shank2^{-/-} ($n=17$) compared to WT ($n=16$) ($P=0.0023$, MWU-test) indicating repetitive decision-making. Data are presented as mean \pm SEM. Single and double asterisks indicate $P<0.05$ and $P<0.01$, respectively. Two-sided t-tests were used, unless stated otherwise.

performance as assessed by the Erasmus Ladder (Baudouin et al 2012). A more recent model examining the 15q11-13 duplication ASD syndrome demonstrated impaired cerebellar synaptic plasticity and motor learning deficits as assessed by eye-blink conditioning (Piochon et al 2014). Perhaps the most definitive study implicating cerebellar dysfunction as etiologic for ASD-like behaviour involved a Purkinje cell-specific deletion of *Tsc1* (Tsai et al 2012). This study was the first to demonstrate that Purkinje cell-specific deletion of an ASD-associated gene results in ASD-like behaviour. Finally, a very recent study using multiple mouse models of syndromic ASD found a consistent pattern of impaired sensorimotor integration (Kloth et al 2015). These studies have established the foundation by which the cerebellar synaptic pathophysiology underlying ASD can be mechanistically investigated (Zoghbi & Bear 2012).

Given the general importance of Shank2 in the regulation of neuronal plasticity (Schmeisser et al 2012, Won et al 2012), we investigated both synaptic and intrinsic plasticity of cerebellar Purkinje cells (Fig. 4). Our results indicate that Shank2 is crucial for PF-PC LTP, but not LTD. Additionally, we show that Shank2 is important for intrinsic plasticity of neuronal excitability (Belmeguenai et al 2010). In contrast to a recent study of the 15q11-13 duplication ASD syndrome in which PC synaptic plasticity deficits were limited to LTD (Piochon et al 2014), our results now highlight LTP impairments as a candidate mechanism underlying the cerebellar pathophysiology of ASD. Shank2 is a dedicated scaffolding protein, which has a major role in the regulation of glutamate receptor integration, synaptic transmission and plasticity (Grabrucker et al 2011, Jiang & Ehlers 2013). Future molecular and functional studies will have to elucidate the exact mechanisms by which Shank2 mediates plasticity in the Purkinje cell, but it may well include a suboptimal integration of GluR subunits as the expression levels of GluA1 and GluA2 were both reduced in the Shank2^{-/-} mice. Since GluR subunit levels were analysed in synaptosomes from whole cerebella, it remains to be further investigated to what extent these changes are limited to the PF to PC synapse.

Because of the cerebellar physiological impairments and the previously reported motor hyperactivity in Shank2^{-/-} mice (Schmeisser et al 2012, Won et al 2012), we examined activity levels during both baseline exploration and motor learning. To our surprise we did not find motor performance abnormalities in the PC-specific L7-Shank2^{-/-} mice during various assessments including five separate locomotion and eye movement tests (Supplementary Fig. 2). However, we did observe substantial impairments of cerebellar motor learning including conditioning of locomotion and eyeblink responses as well as adaptation of compensatory eye movements (Fig. 6). It might seem counterintuitive that baseline motor performance can be intact while the capacity for motor learning is reduced, but this combination has been observed in many different mutant lines over the last few decades (De Zeeuw et al 2011). Most likely, it reflects the indispensable role of PC plasticity for the acquisition of new behaviours within relatively short periods of time as occurs during the experimental training paradigms (i.e. in the order of hours) and the ability of the motor performance control system to compensate upstream and/or downstream of the affected synapse when prolonged adaptation periods are available as occurs during postnatal development (i.e. in the order of weeks) (van Alphen & De Zeeuw 2002). The potential causality of the identified electrophysiological abnormalities as underlying the motor learning impairments is strengthened by our independent findings in another Purkinje cell-specific mouse mutant (L7-PP2B^{-/-}), in which also both synaptic LTP and intrinsic plasticity were affected (Schonewille et al 2010). Together, these phenotypes point towards a PC-dependent contribution to the behavioural motor impairments frequently observed in ASD.

In addition to changes in plasticity, we also found that inhibition of PCs was enhanced in the global Shank2^{-/-} mutants. Since reduced inhibition of PCs increases regularity of SS activity (Wulff et al 2009),

we hypothesized that PCs of the global *Shank2^{-/-}* mutants should have a higher level of irregularity of SS firing (Fig. 3). Indeed, this hypothesis was not only consistent with the *in vivo* extracellular recordings in lobule X of the global *Shank2^{-/-}*, but also confirmed in three different areas (Lobules I-V, Lobules IX-X and the flocculus) of the *L7-Shank2^{-/-}* mice (Fig. 7). Moreover, this correlation was also in line with the fact that the differences in sIPSCs, CV and CV2 had bigger effect sizes in the posterior lobules than the anterior lobules.

The increased frequency of inhibition in the global *Shank2^{-/-}* did not occur concomitantly with increased amplitude of sIPSCs postsynaptically at PCs, indicating that the observed effect could be of pre-synaptic origin. The PC irregularity in the *L7-Shank2^{-/-}* would then have to originate from a pre-synaptic effect of the postsynaptic absence of Shank2. Indeed, recent evidence indicates the possibility of Shank-mediated transsynaptic signalling through transmembrane proteins affecting both post and pre-synaptic processes important for vesicle release probability (Arons et al 2012). This type of transsynaptic signalling could manipulate the inhibitory input to PCs either directly or indirectly, e.g. through altered glutamate spillover from the climbing fiber to Purkinje cell synapse (Szapiro & Barbour 2007). Future research aimed at pinpointing the sites relevant to the effects described above should thus focus not only on Purkinje cell specific mouse mutants, but also on those in which their afferents are specifically affected (Badura et al 2013, Galliano et al 2013a). In doing so, important consideration in studies implementing cell-specific deletions should be given to germline analyses, given the sensitivity of the *L7-cre* (Barski et al 2000, Tsai et al 2012) and *Shank2* lines (Supplementary Table 1) (Kobayashi & Hensch 2013, Schmidt-Suppran & Rajewsky 2007).

We observed a significant decrease in SS frequency in the anterior lobules of global *Shank2^{-/-}* mice, but not in their posterior lobules, nor in the anterior or posterior lobules of *L7-Shank2^{-/-}* mice. We believe that this inconsistency may reflect the fact that the spontaneous SS firing frequency of PCs is probably largely due to their intrinsic properties rather than the synaptic efficacy of their inhibitory or excitatory inputs (Zhou et al 2014). Indeed, blocking inhibitory or excitatory synaptic input to PCs by deleting their GABA-A-gamma2 receptor-subunits or abolishing voltage gated calcium channels at their parallel fiber input primarily affects the regularity of SS firing, rather than their firing frequency (Galliano et al 2013a, Wulff et al 2009). Thus, the consistent irregularity of SS in PCs, particularly in the posterior lobe, of the *Shank2^{-/-}* mutants underlines the putative importance of precise SS regularity for behavioural output (De Zeeuw et al 2011). Although abnormalities in the anterior and posterior lobules have both been proposed as relevant sites of cerebellar pathology in ASD (Mosconi et al 2015), our converging data obtained in the posterior lobe suggest that the mechanisms governing the regularity of SS firing reveal a common biological vulnerability in the etiology of ASD.

Here, we report impaired social and task specific repetitive behaviour due to the Purkinje cell-specific deletion of *Shank2* (Fig. 8). This result is particularly interesting as, to our knowledge, it is the first Purkinje cell-specific mouse model for a non-syndromic form of autism in which ASD-like behaviour has been established. The impaired social behaviour, late-onset ataxia and reduced excitability of Purkinje cells previously observed in *L7-Tsc1* mice (Tsai et al 2012) were due to the absence of a protein that inhibits mTOR signalling through which the translation of a wide variety of proteins is regulated. In contrast, we here show that disruption of the synapse through the absence of a single postsynaptic scaffolding protein in the Purkinje cell is sufficient to show impaired ASD-related motor learning and social behavioural impairments. In addition to the social impairments, we found signs of enhanced repetitive behaviour in the T-maze paradigm, but not the marble burying task or grooming tasks. Since the T-maze task reveals the level of cognitive inflexibility following decision making over consecutive trials rather than the level of repetitious behaviour dominated by high-frequency motor activity that

characterizes the other two tasks and that may well be confounded by deficits in cerebellar motor learning, these results highlight the importance of the Purkinje cell synaptic function for ASD beyond the classically ascribed motor-related behaviour.

One of the main challenges remaining is to mechanistically explain the contribution of impaired Purkinje cell physiology to the observed ASD behavioural phenotypes. As previously mentioned, the Shank family of postsynaptic scaffolding proteins has many different interacting proteins in the postsynaptic density through which they could contribute to the functional establishment of regulatory mechanisms for plasticity. The translational challenge from synapse to behaviour brings about two main questions: How does an impaired Purkinje cell mediate ASD-related behaviour? And how might Purkinje cell impairments lead to abnormal brain function beyond the cerebellum with regards to neurodevelopmental critical periods? The first question has been extensively addressed by the accumulating evidence regarding the contribution of ASD-related cerebellar dysfunction to impaired motor learning, as apparent from the eye movement adaptation, ErasmusLadder, and eyeblink conditioning findings examined here and by other investigators [Kloth et al 2015]. It is indeed possible that the increased inhibition and irregularity of SS firing, in addition to impaired cerebellar plasticity mechanisms, may contribute to social and repetitive behaviour-related phenotypes in ASD. We believe that the answer to how the cerebellum can essentially contribute to socially impaired behaviour could reside in various mechanisms. The idea that disruption of a certain brain area during development could affect the development and consequently the function of other inter-connected areas, also termed developmental diaschisis, has recently been put forward as a prime mechanism for the cerebellum in its ability to influence other cortical areas in critical developmental periods [Wang et al 2014]. In the future, the latter hypothesis can for example be tested with Purkinje cell specific Shank2 ablation at different stages during development using inducible mouse models, as has recently been employed for other ASD-related genes [Mei et al 2016, Silva-Santos et al 2015]. These experiments will help to further elucidate the mechanisms by which differential genes, such as Shank2, regulate cerebellar function and ultimately ASD-like behaviour.

Methods

Experiments and analyses were performed with the experimenters blinded to the genotype. Mice used were global germ-line Shank2^{-/-} and their littermate WTs all bred on a mixed C57BL6/N and C57BL6/J background. The generation of these mice has previously been described in detail [Schmeisser et al 2012, Won et al 2012]. The L7-Shank2^{-/-} was generated by crossing Purkinje specific L7(Pcp2)-Cre [Barski et al 2000] with Shank2^{flxd/flxd} [Schmeisser et al 2012]. Genotyping was performed on postnatal day (P) 7-10 using primers 1700 S (TCCATGGTT TCGCAGAGCG), 1842 AS (TCCCTATTGGGACGCACTGG) and 2394 AS (CAGCATCATGACAATGTCTCCA). For all experiments we used mice from both genders, unless indicated otherwise. The mice were individually housed with food and water available ad libitum and in 12:12 hrs light/dark cycles. All experiments were approved by local and national ethical committees.

Primary antibodies

The anti-Shank2 SA5193 antibody has been characterized previously [Schmeisser et al 2012] the following antibodies were from commercial suppliers: anti-GluA1 [Cat. No. 182 003], anti-GluA2 [Cat. No. 182 103], anti-Nlgn3 [Cat. No. 129 113] [all Synaptic Systems, Goettingen, Germany], anti-3-Tubulin [Cat. No. MRB-435P] [Covance, Brussels, Belgium] and Aldolase C [Cat. No. 12065] [Santa Cruz, Dallas, U.S.A.]

Golgi stainings

Adult mouse cerebella were dissected and prepared using the FD Rapid GolgiStain Kit (NeuroTechnologies, Vilnius, Lithuania). Serial coronal sections of 150 μm were collected from WTs and global Shank2^{-/-} mice and Z-stack images were taken using an upright Axioscope (Carl Zeiss, Jena, Germany). Distal dendrites of Purkinje cells were traced for spine analysis.

Electron microscopy

Adult mice were transcardially perfused with fixative (2 % paraformaldehyde, 2.5 % glutaraldehyde, 1 % saccharose in 0.1 M cacodylate buffer, pH 7.3) and their cerebella were dissected and post-fixed overnight at 4 °C. After dehydration and staining with 2 % uranyl acetate, the material was embedded in epoxy resin. Ultrathin sections were cut using an ultramicrotome (Ultracut UCT, Leica). After lead citrate staining, sections from WTs and global Shank2^{-/-} mice were examined using an electron microscope (JEM 1400 TEM, Jeol). For ultrastructural PSD analysis, spine synapses have been selected in the distal molecular layer where the parallel fiber-Purkinje cell (PF-PC) contacts greatly outnumber other types of synapses.

Biochemistry

Adult mouse cerebella were homogenized on ice in HEPES-buffered sucrose (320 mM sucrose, 5 mM HEPES, pH 7.4) containing protease inhibitor mixture (Roche, Mannheim, Germany). The homogenate was centrifuged (1.000 x g, 4 °C) to remove cell debris and nuclei. The supernatant was further centrifuged (12.000 x g, 4 °C) to obtain a pellet containing the cerebellar synaptosomes. Equal amounts of 10-20 μg protein per lane were separated by SDS-polyacrylamide gel electrophoresis and blotted onto polyvinylidene fluoride membranes using standard protocols. After incubation with primary antibodies (1:1.000 for anti-Shank1, anti-GluA1, anti-GluA2, anti Nlgn3; 1:10.000 for anti- β 3-Tubulin), immunoreactivity was visualized on X-ray film (GE Healthcare, Freiburg, Germany) using HRP-conjugated secondary antibodies (Dako; Hamburg, Germany) and the SuperSignal detection system (Thermo Scientific). For quantification, the films were scanned, the grey value of each band was analysed by ImageJ (National Institutes of Health, Bethesda, MD, USA) and normalized to the grey value of β 3-Tubulin.

Immunohistochemistry

Mouse brains were snap-frozen after removal without perfusion. Tissue was sectioned at 7 μm using a cryostat at -20°C and a knife temperature of -14°C. Sections were air-dried on superfrost glass and stored at -80°C. For staining sections were defrosted at room temperature (RT) for 60 min and subsequently washed with -20°C MeOH for 3 min followed by 3X 10 min of PBS wash. To permeabilize membranes, sections were incubated for 60 min in 0.5% Triton X-100 in PBS at RT and washed 3X in PBS for 10 min. Following a 60 min incubation in 5% BSA (in PBS) at RT and subsequent PBS washing, sections were incubated in SA5193 antibody (1:1000, dissolved in 2% bovine-serum albumin, see [Boeckers et al 1999a]) O/N at 4°C. The sections were then washed for 3X 10 minutes in PBS followed by 120 min of fluorescent antibody staining (1:200, Donkey anti goat-Cy3) in 2% BSA at RT. After the fluorescent antibody a wash of 3X 10 min of PBS was followed by 2X 10 min wash with PB. The sections were then put for 10 min in DAPI (200 μl in 50 ml 0.1 M PB). This was concluded by a 2x 10 min PB wash. For Zebrin (Adolase C) we used a different approach after the defrosting of sections at RT. These slices were washed with 10 min 4% PFA followed by 20 min of methanol and subsequently

by 2 min PBS and 30 min 100 ml PBS (with 2 ml 30% H_2O_2 + 0.8 ml sodium azide). Here after a wash of 2 min PBS and 2X 2 min in PBS (with 1 L PBS, 5 g protifar and 1.5 g glycine, sections were incubated in the primary antibody for Adolase C (1:1000; Santa Cruz, Dallas, U.S.A., Cat. No. 12065) 0/N at 4°C. The sections were then washed for 3X 10 minutes in PBS followed by 90 min of fluorescent antibody staining (1:200, donkey anti goat-Cy3; The Jackson Laboratory, Sacramento, U.S.A., Cat. No 705-165-147) in 2% BSA at RT. After the fluorescent antibody a wash of 3X 10 min of PBS was followed by 2X 10 min wash with PB. The sections were then put for 10 min in DAPI (ThermoFisher Scientific, Waltham, U.S.A., Cat. No. D3571; 200 μ l in 50 ml 0.1 M PB). This was concluded by a 2X 10 min PB wash. Following PBS washing, the sections were thionin-stained and permount-covered using standard protocols. All immunohistological stainings have successfully been replicated on multiple occasions.

Ex vivo electrophysiology

Following decapitation of mice under isoflurane anaesthesia, the cerebellum was removed into an ice-cold 'slicing medium', containing (in mM) 240 sucrose, 2.5 KCL, 1.25 Na_2HPO_4 , 2 $MgSO_4$, 1 $CaCl_2$, 26 $NaHCO_3$ and 10 D-Glucose, that was carbogenated continuously (95% O_2 and 5% CO_2). Sagittal slices, 250 μ m thick, of the cerebellar vermis were cut using a vibrotome (VT1200S, Leica) and put in carbogenated artificial cerebrospinal fluid (ACSF) containing (in mM): 124 NaCl, 5 KCL, 1.25 Na_2HPO_4 , 2 $MgSO_4$, 2 $CaCl_2$, 26 $NaHCO_3$ and 20 D-Glucose, for at least one hour at $34 \pm 1^\circ C$ before the start of the experiment. Slice physiology was done at room temperature $21 \pm 1^\circ C$ or $33 \pm 1^\circ C$ as indicated in the results section and in the presence of 100 μ M picrotoxin except for the sIPSCs recordings. Whole-cell patch clamp recording were performed with an EPC9 amplifier (HEKA Electronics, Lambrecht, Germany). Recordings were excluded if the series (Rs) or input resistances (Ri) changed by more than 15% during the experiment, which was determined using a hyperpolarizing voltage step relative to the -65 mV holding potential. Data analysis (rise times (10-90% for EPSC and action potentials)), decay time (τ) for EPSC and IPSC amplitudes, action potential threshold (identified by steepest slope in membrane potential prior to action potential) and AHP amplitude (minimal membrane potential relative to the action potential threshold) was performed using Clampfit software (Molecular Devices).

For whole-cell recordings Purkinje cells (PCs) were visualized using an upright microscope (Axioskop 2 FS, Carl Zeiss) equipped with a 40X objective. Recording electrodes (3-5 M Ω , 1.65 mm OD and 1.11 mm ID, World Precision Instruments, Sarasota, FL, USA) were filled with an intracellular solution containing (mM): 120 K-Gluconate, 9 KCL, 10 KOH, 4 NaCL, 10 HEPES, 28.5 Sucrose, 4 Na_2ATP , 0.4 Na_3GTP (pH 7.25-7.35 with an osmolality of 295 ± 5). Note that we adjusted the osmolality using sucrose (Belmeguenai et al 2010, Coesmans et al 2004). For the recording of sIPSCs we used an intracellular solution containing (mM): 150 CsCl, 1.5 $MgCl_2$, 0.5 EGTA, 4 Na_2ATP , 0.4 Na_3GTP , 10 HEPES, 5 QX314 (pH 7.25-7.35 with an osmolality of 295 ± 5). For extracellular stimulation of parallel fibers (PFs), similar patch electrodes were filled with ACSF and positioned in the upper third of the molecular layer lateral to the patched Purkinje cell. The stimulation intensity was set to evoke an EPSC of 300 ± 50 pA (typically 3-6 μ A stimulation intensity). For PF-PC transmission we used various inter-stimulus intervals (50-200 ms) (see Fig. 2). For recordings of spontaneously occurring IPSCs (sIPSCs) we used the previously mentioned K^+ -based internal and recorded their occurrence during at least 120 s.

For climbing fiber stimulation similar electrodes (filled with ACSF) were positioned near the patched Purkinje cell soma in the surrounding granule layer. We selected those recordings in which climbing fiber stimuli elicited clear all-or-none responses and lacked the co-activation of Purkinje cell axons (identifiable by backpropagating action potentials) for further analysis. For CF elimination

experimental tissue was prepared in a similar way for all age groups. We systematically scanned the granule cell layer to elicit CF responses and recorded PC responses (using an intracellular solution containing (in mM): 115 CsMeO₃, 20 CsCl, 2.5 MgCl₂, 10 HEPES, 0.6 EGTA, 4 Na₂ATP, 0.4 Na₃GTP, 10 Na-phosphocreatine) at -20 mV holding potential to prevent voltage escape during the CF-responses. For CF-PC transmission we evaluated the paired pulse ratio at 50 ms stimulus interval. To evaluate the complex spike waveforms we analysed the amplitude of the Na⁺-spike and the amplitude of the first Ca²⁺-spikelet evoked during the LTD-tetanus (van Woerden et al 2009). Current clamp recordings were corrected off-line for the calculated liquid junction potential (-10.2 mV).

The synaptic (LTP, LTD) and intrinsic plasticity protocols were recorded from lobules 5/6 and conducted as described previously (Belmeguenai et al 2010, Schonewille et al 2010). In short, for synaptic plasticity all recordings were done in voltage-clamp, except for the tetanus, which consisted of single-pulsed PF-stimulation at 1 Hz for 5 min (LTP) or single-pulsed PF + single-pulsed CF stimulation (5 ms interval) at 1 Hz for 5 min (LTD). We evaluated the synaptic plasticity by the change in PF-EPSC (presented at 0.05 Hz) relative to the mean value calculated during the last 5 min pre-tetanus. For intrinsic plasticity we utilized the PF-LTP tetanus (but without bias currents, i.e., I=0 pA) and evaluated the impact on the number of action potentials evoked by 300 pA current injections during 500 ms (presented at 0.05 Hz).

Extracellular Purkinje cell recordings

In vivo recordings were performed as recently described (Zhou et al 2014). An immobilizing pedestal was fixed on the skull and a craniotomy (Ø 3 mm) was performed on the occipital bone. After recovery of 5 days, mice were head-fixed and body restrained for recordings. Single unit recording was identified by the presence of a short simple spike pause (>6 ms) after each complex spike. Purkinje cells were recorded from vermal lobules I-V and X using single barrel (2.0 mm OD, 1.16 mm ID, Harvard Apparatus, MA, USA) and double barrel (theta septum, 1.5 OD, 1.02 ID; World Precision Instruments) borosilicate glass pipettes. In vivo recordings were analysed offline using Spiketrain (Neurasmus BV, Rotterdam, The Netherlands, www.neurasmus.com) and custom scripts in MatLab (Mathworks, Natick, MA, USA). The CV is calculated by dividing the SD by the mean of the interspike intervals, whereas CV2 is calculated as $2 * I \text{ ISIn} + 1 - \text{ISIn} I / (\text{ISIn} + 1 + \text{ISIn})$.

Compensatory eye movements

Mice between 8 and 10 weeks of age were prepared for head-restrained recordings of compensatory eye movements. These types of recordings have been described in detail previously (Schonewille et al 2010). In order to head restrain the mice during the eye movement task, a small pedestal was attached using Optibond primer and adhesive (Kerr, Bioggio, Switzerland) under isoflurane anaesthesia in O₂ (induction with 4% and maintained at 1.5% concentration). After a recovery period of two to three days, mice were head-restrained by fixation using the pedestal in the experimental setup. A round screen with a random dotted pattern ('drum') surrounded the mouse during the experiment. The optokinetic reflex (OKR), vestibulo-ocular reflex (VOR) and the light-guided vestibulo-ocular reflex (VVOR) were induced using a sinusoidal rotation of the drum in light (OKR), rotation of the table in the dark (VOR) or the rotation of the table (VVOR) in the light. The motor behaviour was assessed by rotating the table and/or drum at 0.1 to 1 Hz with a fixed 5° amplitude. In order to evaluate motor learning, a mismatch between visual and vestibular input was created. Rotating both the visual and vestibular stimuli in phase (at the same amplitude) induced a decrease of gain; rotating the drum at greater amplitude relative to

the table induced the so-called phase reversal of the VOR (day 1, 5° phase difference; day 2, 7.5°; day 3-4, 10°). Rotating the visual and vestibular stimuli out of phase (at the same amplitude) induced the VOR gain increase. All training protocols were induced at 0.6 Hz with table rotation amplitude of 5°. For eye illumination during the experiments two table-fixed infrared emitters (output 600 mW, dispersion angle 7°, peak wavelength 880 nm) and a third emitter, which produced the tracked corneal reflection (CR), were mounted to the camera and aligned horizontally with the optical axis of the camera. Eye movements were recorded with eye-tracking software (ETL-200, ISCAN systems, Burlington, NA, USA). Gain and phase values of eye movements were calculated using Matlab (MathWorks).

Eyeblink conditioning

Mice of 12-15 weeks of age were prepared for head-restrained eyeblink conditioning (ten Brinke et al 2015). In short, a small brass pedestal was attached to the skull using Optibond primer and adhesive (Kerr) and Charisma (Heraeus Kulzer, Armonk, NY, USA), under isoflurane anaesthesia. Three to five days after surgery, mice were habituated during two short (30-45 min) sessions on two days in a sound- and light-isolating chamber which houses the eyeblink set up. During these sessions mice were head-fixed and suspended over a foam cylindrical treadmill. While no stimuli were presented, a 27.5 gauge needle through which US air-puffs are delivered was positioned at 5 mm from the center of the left cornea, a green LED (ø 5 mm) that delivers the CS was placed 5 cm in front of the mouse, and an GMR magnetometer (NVE, Eden Prairie, MN, USA) was fixed above the left eye. During five subsequent acquisition training days, this sensor measured the distance of a miniscule magnet (1.5x0.7x0.5 mm) that was placed on the left lower eyelid with high accuracy, while 200 paired trials were presented, usually spaced 10 ± 2 s apart, plus the time needed for a sporadic unstable eyelid to stabilize in open position. Each paired trial consisted of a 280 ms green LED CS, co-terminating with a 30 ms airpuff (30 psi, through an MPPI-3 pressure injector; ASI, Eugene, OR, USA). All experiments were performed at approximately the same time of day by the same experimenter. Individual eyeblink traces were analyzed using custom LabVIEW (National Instruments, Austin, TX, USA) or MATLAB (Mathworks, Natick, MA, USA) scripts. Trials with significant activity in a 500 ms pre-CS baseline period were regarded as invalid for further analysis. Valid trials were aligned by making the mean of their baseline activity zero, and the average amplitude of all post-US unconditioned blink responses was used to denote 100% eyelid closure. From this, the average eyelid closure as a percentage from baseline to full closure at the end of the CS-US interval was calculated over all valid trials. To calculate percentage of CRs, trials were judged to contain a CR if the eye closed for more than 5% between 50-250 ms after CS and the CR reached its peak after 100 ms.

ErasmusLadder

The ErasmusLadder (Noldus, Wageningen, Netherlands) is a fully automated system consisting of a horizontal ladder between two shelter boxes. It has 37 rungs on each side, spaced 15 mm apart, and attached to custom-made pressure sensors that are continuously monitored. In order to create a left-right alternating pattern, even rungs on one side and odd rungs on the other side are elevated by 6 mm. Prototype testing revealed that optimum forepaw displacement for mice is about 6 cm in a single step at medium high velocity, which is the distance between 3 consecutive elevated rungs and is defined as efficient step in the text (for more details, see (Veloz et al 2014)). It is clear from previous studies that mice improve their walking efficiency over training sessions by increasing the number of efficient steps relative to steps of lower sizes (Veloz et al 2014). In the current study, mice (male, 15-18 weeks old) were tested in 6 daily sessions consisting of 2 unperturbed sessions, 1 session with

a fixed obstacle in the middle of the ladder and 3 perturbed sessions. During the first three sessions, mice were trained to walk between two shelter boxes for 50 trials each day. In the perturbed sessions, a sudden appearance of a rising rung on the right side of the mouse was used as the unconditional stimulus (US). A 15 kHz tone was used as the conditional stimulus (CS) and preceded the US by 200 ms in CS-US paired trials. CS-only trials and paired trials were randomly distributed among 50 trials. There were twice as many paired trials as CS-only trials. Step length and step time were defined as the distance and time between two consecutive touches from the right front limb. To estimate motor adaptation in CS-only trials, we calculated step speed (step length/step time) using only the steps within 1 s before and 1 s after the CS. The speed ratio during conditioning was defined as the speed post-CS divided by the speed pre-CS.

General behavioural analyses

Behavioural experiments were performed using L7-Shank2^{-/-} and WT littermate controls aged 8-16 weeks during the light period of their diurnal cycle. The mice used in the general behavioural experiments described here underwent multiple tests.

For the PhenoTyper test, mice were placed in a homecage-like apparatus (Noldus) with ad libitum access to food and water, and left to explore for 30 minutes. Locomotion was recorded using the automated software Noldus Ethovision XT 11 and distance and speed were calculated.

For the open field test, mice were placed in a novel circular, brightly-lit 110-cm-diameter open arena for 10 min. Locomotion was recorded using the automated software Noldus Ethovision XT 11 and total distance travelled, as well as average speed were calculated. During analysis the arena was subdivided in three concentric zones named the inner (25 cm), middle (15 cm) and outer zone (15 cm), and percentage of time in each zone was calculated.

For the three-chamber social interaction test, age and gender-matched WT target subjects (Stranger 1 and 2) were habituated for 5 consecutive days before beginning of testing by being placed inside round metal-wired cages. On the test day, experimental mice were placed in the central chamber of a clear Plexiglas box (60 x 35 cm) divided into three interconnected chambers. After habituation for 5 min. an unfamiliar mouse (Stranger 1; S1) was introduced into a wire cage in one of the side-chambers and an empty wire cage in the other side-chamber. The dividers were then raised and the test mouse was allowed to freely explore all three chambers over a 5-minute session. Next, the mouse remained in the chamber with stranger 1 for an additional 5-minute session. Subsequently, a novel stranger mouse (Stranger 2; S2) was placed in the previously empty wire cage and again the test mouse was left to explore for 5 min. Time spent in each chamber, as well as overall locomotion, was calculated using the automated software Noldus Ethovision XT 11. Preference indices were calculated by subtracting the time spent with the empty wire cage from the time spent with stranger 1 (S1 – E), and subtracting the time spent with stranger 1 from time spent with stranger 2 (S2 – S1).

For the T-maze spontaneous alternation test, mice were placed at the base of a T-maze (arm length 50 cm) and were given the choice to freely explore either the right or left arm of the maze for 10 consecutive trials. A choice was assumed to be made when mice stepped into an arm with all four paws. At that moment the gate to that arm was closed and the animal was allowed to explore the arm for 5 s. Then, the mouse was gently placed back at the base of the T-maze for the next trial. When the mouse chose a similar arm at two consecutive trials, this was scored as number of repeats, indicative of repetitive behaviour.

For the grooming test, mice were removed from their homecage, received a single puff of water spray and placed in clean transparent cages (15 x 15 x 20 cm) under bright light for 15 min. Behaviour was recorded with a high-speed camera (30Hz full frame rate), and time spent grooming was scored by two independent raters. All types of grooming – paw licking, nose and head self-grooming, body grooming, leg grooming and tail/genital grooming – were scored.

For the marble burying test, Makrolon cages (50 x 26 x 18 cm) were filled with 4 cm of bedding material and 20 glass marbles, which were arranged in an equidistant 4 x 5 grid. Animals were given access to the marbles for 30 min. Marbles 100% covered by bedding were scored as buried and marbles covered partially contributed 50% to the total score.

For the olfactory test, a piece (1.25 g) of cookie was put into the subject's cage each day for three consecutive days, and checked for complete consumption the following day. For 24 hrs before the test phase, mice were completely food-deprived. Subjects were placed in a clean Makrolon cage (50 x 26 x 18 cm) with 4 cm of clean bedding, and allowed to habituate for 5 min. Then, a piece of cookie (1.25 g) was hidden in a random corner in the cage at 1 cm depth. Latency to find the cookie was recorded for a maximum of 15 mins (900 s).

Data analysis

In the text, mean \pm SD values are presented, in the figures SEM-values are reported, and p-values smaller than 0.05 are considered significantly different. Two-sided Student's t-tests were performed, unless stated otherwise. For a complete representation of the data we have included a detailed overview of all statistics in Supplementary Table 1. Additionally, since the L7-Cre line was shown to reveal germline deletions [see also [44]] and since the potential impact of cerebellar Purkinje cells on general cognitive tests is widely debated [Galliano et al 2013b, Rochefort et al 2011], we have checked for heterozygous germline deletions in our L7-Shank2 mice and statistically excluded the possibility they could have influenced our conclusions on the non-cerebellar paradigms (Supplementary Table 1).

References

- Allen G. 2005. The cerebellum in autism. *Clinical Neuropsychiatry* 2: 321-37
- Arons MH, Thynne CJ, Grabrucker AM, Li D, Schoen M, et al. 2012. Autism-associated mutations in ProSAP2/Shank3 impair synaptic transmission and neurexin-neuroligin-mediated transsynaptic signaling. *J Neurosci* 32: 14966-78
- Badura A, Schonewille M, Voges K, Galliano E, Renier N, et al. 2013. Climbing fiber input shapes reciprocity of Purkinje cell firing. *Neuron* 78: 700-13
- Bailey A, Luthert P, Dean A, Harding B, Janota I, et al. 1998. A clinicopathological study of autism. *Brain* 121: 889-905
- Barski JJ, Dethleffsen K, Meyer M. 2000. Cre recombinase expression in cerebellar Purkinje cells. *genesis* 28: 93-98
- Baudouin SJ, Gaudias J, Gerharz S, Hatstatt L, Zhou K, et al. 2012. Shared synaptic pathophysiology in syndromic and nonsyndromic rodent models of autism. *Science* 338: 128-32
- Becker EB, Stoodley CJ. 2013. Autism spectrum disorder and the cerebellum. *International review of neurobiology* 113: 1
- Belmeguenai A, Hosy E, Bengtsson F, Pedroarena CM, Piochon C, et al. 2010. Intrinsic plasticity complements long-term potentiation in parallel fiber input gain control in cerebellar Purkinje cells. *The Journal of neuroscience* 30: 13630-43
- Berkel S, Marshall CR, Weiss B, Howe J, Roeth R, et al. 2010. Mutations in the SHANK2 synaptic scaffolding gene in autism spectrum disorder and mental retardation. *Nature genetics* 42: 489-91
- Böckers TM, Segger-Junius M, Iglaue P, Bockmann J, Gundelfinger ED, et al. 2004. Differential expression and dendritic transcript localization of Shank family members: identification of a dendritic targeting element in the 3' untranslated region of Shank1 mRNA. *Molecular and Cellular Neuroscience* 26: 182-90
- Boeckers TM, Kreutz MR, Winter C, Zuschratter W, Smalla K-H, et al. 1999a. Proline-rich synapse-associated protein-1/cortactin binding protein 1 (ProSAP1/CortBP1) is a PDZ-domain protein highly enriched in the postsynaptic density. *The Journal of neuroscience* 19: 6506-18
- Boeckers TM, Winter C, Smalla K-H, Kreutz MR, Bockmann J, et al. 1999b. Proline-rich synapse-associated proteins ProSAP1 and ProSAP2 interact with synaptic proteins of the SAPAP/GKAP family. *Biochemical and biophysical research communications* 264: 247-52
- Bourgeron T. 2015. From the genetic architecture to synaptic plasticity in autism spectrum disorder. *Nature Reviews Neuroscience* 16: 551-63
- Chen JA, Peñaarrikano O, Belgard TG, Swarup V, Geschwind DH. 2015. The Emerging Picture of Autism Spectrum Disorder: Genetics and Pathology. *Annual Review of Pathology: Mechanisms of Disease* 10: 111-44
- Coesmans M, Weber JT, De Zeeuw CI, Hansel C. 2004. Bidirectional parallel fiber plasticity in the cerebellum under climbing fiber control. *Neuron* 44: 691-700
- De Zeeuw CI, Hoebeek FE, Bosman LWJ, Schonewille M, Witter L, Koekkoek SK. 2011. Spatiotemporal firing patterns in the cerebellum. *Nature Reviews Neuroscience* 12: 327-44
- De Zeeuw CI, Ten Brinke MM. 2015. Motor Learning and the Cerebellum. *Cold Spring Harbor perspectives in biology* 7: a021683
- Durand CM, Betancur C, Boeckers TM, Bockmann J, Chaste P, et al. 2007. Mutations in the gene encoding the synaptic scaffolding protein SHANK3 are associated with autism spectrum disorders. *Nat Genet* 39: 25-7
- Galliano E, Gao Z, Schonewille M, Todorov B, Simons E, et al. 2013a. Silencing the majority of cerebellar granule cells uncovers their essential role in motor learning and consolidation. *Cell reports* 3: 1239-51
- Galliano E, Potters JW, Elgersma Y, Wisden W, Kushner SA, et al. 2013b. Synaptic transmission and plasticity at inputs to murine cerebellar Purkinje cells are largely dispensable for standard nonmotor tasks. *J Neurosci* 33: 12599-618
- Grabrucker AM, Schmeisser MJ, Schoen M, Boeckers TM. 2011. Postsynaptic ProSAP/Shank scaffolds in the cross-hair of synaptopathies. *Trends in cell biology* 21: 594-603
- Hashimoto K, Kano M. 2003. Functional differentiation of multiple climbing fiber inputs during synapse elimination in the developing cerebellum. *Neuron* 38: 785-96
- Häusser M, Clark BA. 1997. Tonic synaptic inhibition modulates neuronal output pattern and spatiotemporal synaptic integration. *Neuron* 19: 665-78
- Jiang Y-h, Ehlers MD. 2013. Modeling Autism by *SHANK* Gene Mutations in Mice. *Neuron* 78: 8-27
- Kanner L. 1943. Autistic disturbances of affective contact. *Nervous child* 2: 217-50
- Kloth AD, Badura A, Li A, Cherskov A, Connolly SG, et al. 2015. Cerebellar associative sensory learning defects in five mouse autism models. *eLife* 4: e06085
- Kobayashi Y, Hensch TK. 2013. Germline recombination by conditional gene targeting with Parvalbumin-Cre lines. *Front Neural Circuits* 7: 168
- Koekkoek SKE, Yamaguchi K, Milojkovic BA, Dortland BR, Ruigrok TJH, et al. 2005. Deletion of FMR1 in Purkinje cells enhances parallel fiber LTD, enlarges spines, and attenuates cerebellar eyelid conditioning in Fragile X syndrome. *Neuron* 47: 339-52
- Leblond CS, Heinrich J, Delorme R, Proepper C, Betancur C, et al. 2012. Genetic and functional analyses of SHANK2 mutations suggest a multiple hit model of autism spectrum disorders. *PLoS Genet* 8: e1002521
- Leblond CS, Nava C, Polge A, Gauthier J, Huguet G, et al. 2014. Meta-analysis of SHANK mutations in autism spectrum disorders: a gradient of severity in cognitive impairments. *PLoS genetics* 10: e1004580
- Marko MK, Crocetti D, Hulst T, Donchin O, Shadmehr R, Mostofsky SH. 2015. Behavioural and neural basis of anomalous motor learning in children with autism. *Brain* 138: 784-97
- Mei Y, Monteiro P, Zhou Y, Kim JA, Gao X, et al. 2016. Adult restoration of Shank3 expression rescues selective autistic-like phenotypes. *Nature* 530: 481-4
- Memari AH, Ghanouni P, Shayestehfar M, Ghaehri B. 2014. Postural control impairments in individuals with autism spectrum

- disorder: a critical review of current literature. *Asian journal of sports medicine* 5
- Menashe I, Grange P, Larsen EC, Banerjee-Basu S, Mitra PP. 2013. Co-expression profiling of autism genes in the mouse brain. *PLoS computational biology* 9: e1003128
- Mosconi MW, Wang Z, Schmitt LM, Tsai P, Sweeney JA. 2015. The role of cerebellar circuitry alterations in the pathophysiology of autism spectrum disorders. *Frontiers in neuroscience* 9: 296
- Mostofsky SH, Goldberg MC, Landa RJ, Denckla MB. 2000. Evidence for a deficit in procedural learning in children and adolescents with autism: implications for cerebellar contribution. *Journal of the International Neuropsychological Society* 6: 752-59
- Oristaglio J, West SH, Ghaffari M, Lech MS, Verma BR, et al. 2013. Children with autism spectrum disorders show abnormal conditioned response timing on delay, but not trace, eyeblink conditioning. *Neuroscience* 248: 708-18
- Piochon C, Kloth AD, Grasselli G, Titley HK, Nakayama H, et al. 2014. Cerebellar plasticity and motor learning deficits in a copy-number variation mouse model of autism. *Nature communications* 5
- Rocheffort C, Arabo A, Andre M, Poucet B, Save E, Rondi-Reig L. 2011. Cerebellum shapes hippocampal spatial code. *Science* 334: 385-9
- Sala C, Vicidomini C, Bigi I, Mossa A, Verpelli C. 2015. Shank synaptic scaffold proteins: keys to understanding the pathogenesis of autism and other synaptic disorders. *Journal of neurochemistry*
- Sato D, Lionel AC, Leblond CS, Prasad A, Pinto D, et al. 2012. SHANK1 Deletions in Males with Autism Spectrum Disorder. *American journal of human genetics* 90: 879-87
- Schmahmann JD. 2010. The role of the cerebellum in cognition and emotion: personal reflections since 1982 on the dysmetria of thought hypothesis, and its historical evolution from theory to therapy. *Neuropsychology review* 20: 236-60
- Schmeisser MJ, Ey E, Wegener S, Bockmann J, Stempel AV, et al. 2012. Autistic-like behaviours and hyperactivity in mice lacking ProSAP1/Shank2. *Nature* 486: 256-60
- Schmidt-Suppran M, Rajewsky K. 2007. Vagaries of conditional gene targeting. *Nat Immunol* 8: 665-8
- Schmitt LM, Cook EH, Sweeney JA, Mosconi MW. 2014. Saccadic eye movement abnormalities in autism spectrum disorder indicate dysfunctions in cerebellum and brainstem. *Molecular autism* 5: 47
- Schonewille M, Belmeguenai A, Koekkoek SK, Houtman SH, Boele HJ, et al. 2010. Purkinje cell-specific knockout of the protein phosphatase PP2B impairs potentiation and cerebellar motor learning. *Neuron* 67: 618-28
- Sears LL, Finn PR, Steinmetz JE. 1994. Abnormal classical eye-blink conditioning in autism. *Journal of autism and developmental disorders* 24: 737-51
- Silva-Santos S, van Woerden GM, Bruinsma CF, Mientjes E, Jolfaei MA, et al. 2015. Ube3a reinstatement identifies distinct developmental windows in a murine Angelman syndrome model. *The Journal of clinical investigation* 125: 2069-76
- Stins JF, Emck C, de Vries EM, Doop S, Beek PJ. 2015. Attentional and sensory contributions to postural sway in children with autism spectrum disorder. *Gait & Posture*
- Stoodley CJ. 2014. Distinct regions of the cerebellum show gray matter decreases in autism, ADHD, and developmental dyslexia. *Frontiers in systems neuroscience* 8
- Szapiro G, Barbour B. 2007. Multiple climbing fibers signal to molecular layer interneurons exclusively via glutamate spillover. *Nat Neurosci* 10: 735-42
- Takarae Y, Minshew NJ, Luna B, Krisky CM, Sweeney JA. 2004. Pursuit eye movement deficits in autism. *Brain* 127: 2584-94
- ten Brinke MM, Boele HJ, Spanke JK, Potters JW, Kornysheva K, et al. 2015. Evolving Models of Pavlovian Conditioning: Cerebellar Cortical Dynamics in Awake Behaving Mice. *Cell Rep* 13: 1977-88
- Tsai PT, Chu Y, Greene-Colozzi E, Sadowski AR, Leech JM, et al. 2012. Autistic-like behaviour and cerebellar dysfunction in Purkinje cell Tsc1 mutant mice. *Nature* 488: 647-51
- van Alphen AM, De Zeeuw CI. 2002. Cerebellar LTD facilitates but is not essential for long-term adaptation of the vestibulo-ocular reflex. *Eur J Neurosci* 16: 486-90
- van Woerden GM, Hoebeek FE, Gao Z, Nagaraja RY, Hoogenraad CC, et al. 2009. betaCaMKII controls the direction of plasticity at parallel fiber-Purkinje cell synapses. *Nat Neurosci* 12: 823-5
- Veloz MFV, Zhou K, Bosman LWJ, Potters J-W, Negrello M, et al. 2014. Cerebellar control of gait and interlimb coordination. *Brain Structure and Function*: 1-24
- Wang SSH, Kloth AD, Badura A. 2014. The cerebellum, sensitive periods, and autism. *Neuron* 83: 518-32
- Won H, Lee H-R, Gee HY, Mah W, Kim J-I, et al. 2012. Autistic-like social behaviour in Shank2-mutant mice improved by restoring NMDA receptor function. *Nature* 486: 261-65
- Wulff P, Schonewille M, Renzi M, Viltano L, Sassoè-Pognetto M, et al. 2009. Synaptic inhibition of Purkinje cells mediates consolidation of vestibulo-cerebellar motor learning. *Nature neuroscience* 12: 1042-49
- Zhou H, Lin Z, Voges K, Ju C, Gao Z, et al. 2014. Cerebellar modules operate at different frequencies. *eLife*: e02536-e36
- Zoghbi HY, Bear MF. 2012. Synaptic dysfunction in neurodevelopmental disorders associated with autism and intellectual disabilities. *Cold Spring Harbor perspectives in biology* 4: a009886
- Zwaigenbaum L, Bryson S, Garon N. 2013. Early identification of autism spectrum disorders. *Behavioural brain research* 251: 133-46

